

## Full Length Article

# Additive manufacturing of three-dimensional metal-glass functionally gradient material components by laser powder bed fusion with *in situ* powder mixing

Xiaoji Zhang<sup>a</sup>, Yuan-hui Chueh<sup>a</sup>, Chao Wei<sup>a</sup>, Zhe Sun<sup>a</sup>, Jiwang Yan<sup>b</sup>, Lin Li<sup>a,\*</sup>

<sup>a</sup> Laser Processing Research Centre, School of Engineering, Department of Mechanical, Aerospace and Civil Engineering, The University of Manchester, Manchester, M13 9PL, UK

<sup>b</sup> Department of Mechanical Engineering, Faculty of Science and Technology, Keio University, Hiyoshi 3-14-1, Kohoku-ku, Yokohama 223-8522, Japan

## ARTICLE INFO

## Keywords:

Functionally gradient materials  
Powder bed fusion  
Multi-material selective laser melting  
Copper-glass  
Horizontal gradient structure

## ABSTRACT

Existing commercial three-dimensional (3D) printing systems based on powder bed fusion approach can normally only print a single material in each component. In this paper, functionally gradient materials (FGM) with composition variation from a copper alloy to a soda-lime glass were manufactured using a proprietary nozzle-based multi-material selective laser melting (MMSLM) system. An *in situ* powder mixing system was designed to mix both metal and glass powders at selective ratios and the mixed powders were dispensed with an ultrasonic vibration powder feeding system with multiple nozzles. From the cross section analysis of the gradient structures, glass proportion increased gradually from the metallic matrix composite (MMC), transition phase to ceramic matrix composite (CMC). The pure copper alloy joined the MMC part and the pure glass phase penetrated into the CMC part during laser processing, which anchored the glass phase, as the main mechanism of combining pure metal and pure glass by FGM in 3D printed parts. From results of indentation, tensile and shear tests on the gradient material samples, it showed that mechanical properties of the FGM gradually changed from ductility (metal side) to brittle (glass side). The weakest part of the FGM structure occurred at the interface between transition phase and the CMC, which was also the interface between the ductile and brittle phases.

## 1. Introduction

Selective Laser Melting (SLM) or laser powder bed fusion is a significant branch of the Additive Manufacturing (AM) family that can print complex fully dense metallic parts. In order to add more functionality from three-dimensional (3D) printed part, multiple material selective laser melting (MMSLM) was developed in the last decade. Challenges of MMSLM include multi-material delivery, material contamination avoidance, material recycling, new software configuration considering multiple materials, varying process parameters for different materials, effects of one material on the other, and the interfaces between different materials [1]. Multiple powder delivery and varying laser processing parameters for different materials are two major requirements to achieve multi-material SLM. Ultrasonic vibration was effectively applied for point-by-point dispensing of cohesive powders [1–7]. Researchers at The University of Manchester were among the first to demonstrate MMSLM. Al-Jamal et al. achieved laser melting on two-dimensional (2D) multiple metallic powders by dispensing copper

powders and H13 tool steel powders separately using a single ultrasonic vibration actuator [2]. Wei et al. succeeded in combining ultrasonic powder feeding and powder bed spreading to manufacture 3D multiple material metallic parts with discrete interfaces between two types of metallic materials, 316L/In718, and 316L/Cu10Sn [3]. Both investigations used only metallic materials. Ceramics are widely applied in various industries due to their wear resistance, corrosion resistance, preservability, and heat and electrical insulation. Selective laser melting of glass materials, e.g. soda-lime glass [8] and silica [9] was previously reported, which would provide useful references for selecting suitable processing conditions for these materials in the current investigation. Zhang et al., at The University of Manchester previously developed a dual ultrasonic feeding system, which generated stable flow rates of powders to fabricate metal-glass parts by Selective Laser Melting [1]. However, poor bonding between the metal and glass were found from the research. This was because the tension generated by volume shrinkage during cooling would detach the glass from the metal surface.

\* Corresponding author.

E-mail address: [lin.li@manchester.ac.uk](mailto:lin.li@manchester.ac.uk) (L. Li).

<https://doi.org/10.1016/j.addma.2020.101113>

Received 21 June 2019; Received in revised form 26 January 2020; Accepted 5 February 2020

Available online 05 February 2020

2214-8604/ © 2020 Elsevier B.V. All rights reserved.

Challenges of bonding between metal and glass have been investigated in the glass-to-metal sealing-joining technology. One way to improve the bonding of two materials was improving material wetting to reduce contact angles between materials with similar expansion coefficients, such as 7056 glass and kovar alloy [10]. Another method is to generate an oxide layer on the metal surface by pre-oxidation in a furnace, which acts as a bonding between the metal and the glass materials [11,12]. However, match joining (joining two materials with similar expansion coefficients) would limit number of materials in SLM. Therefore, a manufactured transition material is needed to anchor the glass to metal.

For connecting two incompatible materials (metal and ceramic), it was found by Udupa et al. [13] and Howard et al. [14] that functionally gradient materials (FGMs) could act as an interfacial layer to enhance the bond strength. FGMs are high performance, microscopically inhomogeneous materials with engineered gradients of composition and structure with specific properties in the preferred orientation [15]. Ceramic-metal composites were widely applied in FGMs research [16–19], where the ceramic part has good thermal and corrosion resistances and the metallic part provides superior fracture toughness and weldability [20]. The connecting mechanism is that the composition of metal-ceramic FGMs can be gradually changed from pure metallic phase, metallic matrix composite (MMC), transition phase, ceramic matrix composite (CMC) to pure ceramic phase [15,21].

In order to apply MMSLM for FGM component manufacture, two main challenges need to be considered. Firstly, for material delivery, not only stable powder flow rates are necessary, but also *in situ* variations of ratios of the two types of powders are needed in the system. In the research reported by Zhang et al. [1], stable powder flow rates dispensed by a dual ultrasonic vibration feeding system were demonstrated. However, there was no effective system to mix both powders evenly *in situ*. Yang et al. [22] developed a system which could dispense two types of powders with different ratios by sonic vibration. However, the powders could not be mixed evenly by only a static cone hopper. Therefore, it is necessary to develop a feeding system for different mixing ratios of powders *in situ*. Secondly, some forms of chemical reactions between materials may be helpful. The high energy density from a high power laser beam can lead to chemical reactions in materials, which would cause fine and uniform distribution of compounds, better wetting, and release of exothermic energy helpful to binding [21].

In this research, a new, *in situ* powder mixing system was developed that allowed two different powders to be mixed and dispensed in a selective ratio. Cu10Sn copper alloy powders and soda-lime glass powders were used in the research. Optimization of laser fusion parameters for different powder mixing ratios was carried out. Indentation, tensile and shear tests on the composites of Selective Laser Melting at different powder ratios were carried out to examine the mechanical properties. Microstructural analysis was carried out using an SEM and optical microscopy.

## 2. Design of *in situ* powder mixing and feeding system

Different ratios of both metal powders and glass powders were mixed using a designed mixing system and the mixed powders were dispensed with an ultrasonic vibration feeding system. Dual ultrasonic vibration was used for providing stable powder flow rates, especially cohesive powders in a range of 10–50  $\mu\text{m}$ , which was demonstrated in Zhang's previous research [1].

As shown in Fig. 1, powder layers can be deposited with the point-by-point powder feeding system which can dispense different types of powders selectively. Therefore, a 2D pattern in one layer can be formed by different powders. Then the laser selectively scans on the powder layer to melt powders and the melted parts will cool down quickly to form a solid part. After completing a layer, the work platform lowers by a distance equivalent to the thickness one layer and the next layer is

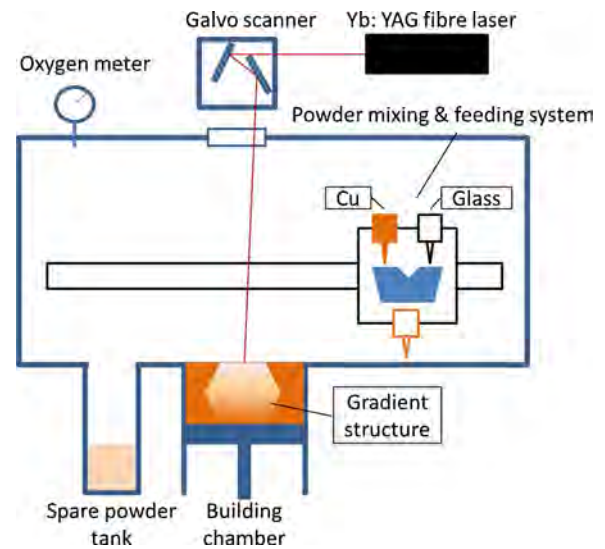


Fig. 1. Schematic of the system structure and processing mechanism.

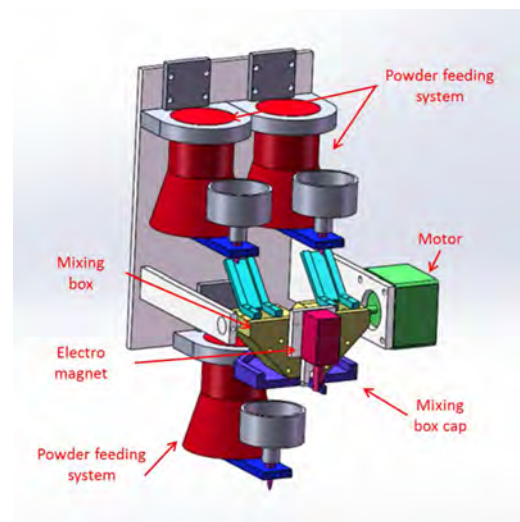


Fig. 2. The detailed structure of the designed mixing system.

formed repeatedly by the feeding system. This procedure was repeated until the 3D printed part was completed.

The core part of the system is the powder mixing and feeding system. As shown in Fig. 2, the system had three sub vibration feeding systems to provide stable powder flow rates. Two upper vibration feeding systems dispensed two different types of powders, metal powders and glass powders, into the lower mixing box with constant powder flow rates. Based on stable flow rates, the amount of powders dispensed could be controlled by dispensing time. According to experimental results of powder flow rates of both powders in Section 4.1, the flow rate was several milligrams per second, which means the dispensing accuracy can be milligram-scale.

Both types of powders could be mixed evenly by rotating the mixing box several times (Fig. 3). The box cap then released the mixture to a lower hopper. The lower feeding system then dispensed powders from the mixing box to the processing platform.

The inner structure of the mixing system is shown in Fig. 4. The aluminium alloy components of the system were manufactured by CNC machining centre with smooth surfaces and the surface roughness  $R_a$  was about 3.2  $\mu\text{m}$ . Therefore, contamination by very few attached powders in the mixing chamber can be ignored. The powders were delivered into the box through a 2 mm-wide channel directly to the

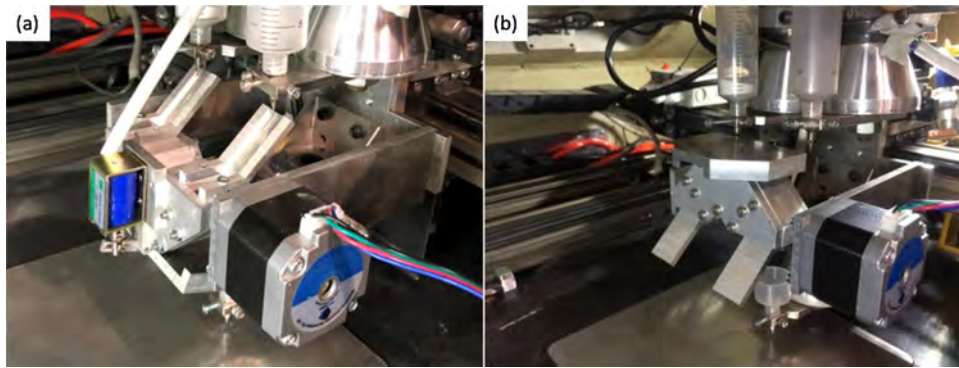


Fig. 3. The powder mixing system; (a) delivering powders into a mixing box and (b) mixing powders by motor controlled rotation of the box.

bottom of the box. Powders were then continuously separated and merged in both horizontal and vertical directions by a rotary motion system driven by an electric motor. Through this, horizontal and vertical mixing enabled the powders to distribute evenly. After rotating several times, the powders in the box were delivered from the exit of the box which was covered by a cap controlled with an electromagnet valve into the lower ultrasonic piezoelectric transducer (PZT) powder feeding system. When a single material was needed, both the upper and the lower feeding systems worked simultaneously without activating the mixing system, so that powders could be directly delivered (Fig. 5). In this case, the whole feeding system played as a dual ultrasonic vibration feeding system.

Due to the differences of Cu10Sn copper and soda-lime glass powders in terms of cohesion and density, enough mixing time is necessary for uniform distribution of both powders. According to the powder distribution of both materials of Section 4.1, it was found 5-minute mixing was enough as the powder mass of every mixing was only about several grams. The rotary speed was 60 r/min for mixing. Flow rates of single type powders and mixed powders were examined with an electronic balance (Ek-300i, A&D Instruments Ltd., Abingdon, Oxfordshire, UK). Based on previous research on ultrasonic vibration dispensing of dry powders, lower vibrational power and relatively larger orifice diameter would be used for stable and constant flow rate feeding, which can also guarantee constant layer thickness along the track [1]. Characteristics of the layer thickness (the deposited line height) were investigated in the previous research by the authors and it was found that generally the layer thickness could be twice or three times of the average powder size [1]. The composition varied from metallic matrix composite (MMC), transition phase, to ceramic matrix composite (CMC) by controlling the dispensing time of the two upper nozzles. The ranges of MMC, transition phase and CMC can be identified according to results shown in Section 4.1. The optimized parameters of the feeding system are shown in Table 1. The traverse speed of the vibrated nozzle during dispensing was 3000 mm/min, the stand-off distance from the nozzle to the working platform was 1 mm, and the hatch distance was 0.5 mm.

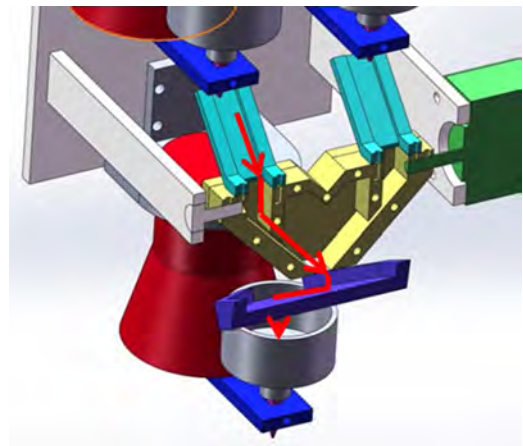


Fig. 5. Schematic of dispensing a single type of powders by the system.

Table 1  
Parameters of the ultrasonic vibration feeding system.

No.	Powder type	Vibrational parameters		Orifice geometry	
		Vibrational frequency (kHz)	Vibrational power (W)	Orifice diameter (mm)	Angle of orifice
Upper PZT 1	Cu10Sn	28	12	0.3	30
Upper PZT 2	Soda-lime	28	12	0.35	30
Lower PZT	Mixture	28	12	0.35	30

### 3. Materials and methods

#### 3.1. Laser device and parameters

A 500 W ytterbium single-mode, continuous wave (CW) fibre laser

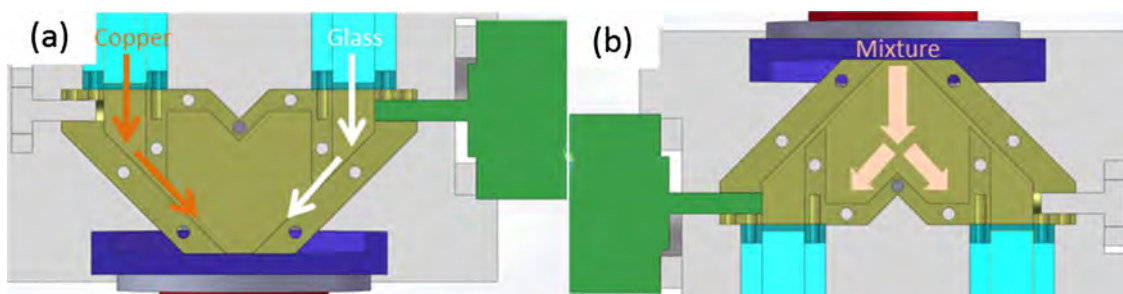


Fig. 4. Mechanism of the mixing system; (a) powders were both vertically and horizontally merged (b) powders were horizontally separated and vertically merged again.

**Table 2**  
Optimized laser parameters on different materials.

Material	Power (W)	Scanning speed (mm/s)	Hatch distance ( $\mu\text{m}$ )
Cu10Sn	125	150	100
Soda-lime glass	100	200	100
Mixtures	100	200	100

(IPG Photonics (UK) Ltd., YLR-500-WC) of a 1070 nm wavelength with an 80  $\mu\text{m}$  focused spot size was scanned over the powder bed in a designed pattern using an Intelli SCAN x-y galvo (SCANLAB GmbH, Puchheim, Germany controlled with software laserDESK. Argon gas was used for gas shield in the sealed chamber during processing. Laser parameters on different ratios of the mixture were optimized as shown in Table 2. The laser parameters for the different compositions were the same because the fusing mechanism was that the laser melts the metal part of the mixture and the heat is transferred to glass powders resulting in fused solid gradient compositions.

Optical microscopes (VHX-5000 and VHX-500 F from KEYENCE Corporation) were used for observing morphological characteristics of the surfaces and cross sections of the samples. Microstructures were observed using scanning electron microscopy (SEM, Zeiss Sigma VP FEG SEM) and the chemical element distribution was measured using energy dispersive spectroscopy (EDS, Oxford Instruments X-max<sup>N</sup> 150).

### 3.2. Powders

As shown in Fig. 6, the Cu10Sn copper-alloy spherical powders of 10–45  $\mu\text{m}$  diameter (Makin Metal Powders Ltd. UK) and spherical soda-lime powders of  $90 \pm 2 \mu\text{m}$  (from Goodfellow Cambridge Ltd., Huntingdon, UK) were used in this investigation. The two types of powders were mixed in various ratios to form gradient materials. Different ratios of glass powders were prepared from 5 wt. % (MMC) to 65 wt. % (CMC) of the mixture with a change of 10 % in each different powder mixture.

### 3.3. Mechanical property testing procedures

In order to understand the mechanical properties of the FGMs, A Durascan-80 hardness tester with a Vickers indenter of 136° diamond pyramid was used to measure the Vickers microhardness on the interfaces between glass and copper of the gradient materials. However, due to the large differences of hardness between the glass and copper alloy, the indenter would slip to the copper side (softer than glass), so that the testing results were not reliable. Therefore, in order to cover the micro-scale interfaces between two materials, the indentation with a higher loading was needed, which cannot be achieved by the micro-indentation machine. Hardness measurements with a Vickers indenter (No. 2005-6608, Calibrations Ltd., UK) and a 30 kg load was carried out on the polished surface of each type of the FGMs as shown in Fig. 7 (a).

The aim of using FGMs in this research was to improve the bonding between dissimilar materials, *i.e.* the copper alloy and soda lime glass. Tensile and shear tests were carried out to evaluate this function. The surface area of the samples was 20 mm x 20 mm. The sample surfaces were polished and connected to a holder using Technic Metacryl glue (Technicqll, 32-540Trzebinia, Poland) of which the average strength was 20–24 MPa. For shear tests, in order to guarantee that the forces were collinear, a special Z-shape holder was used as shown in Fig. 8.

## 4. Results and discussion

### 4.1. Powder mixing and flow rate characteristics

Particular ratios of the powder mixture can be controlled by the dispensing time of the copper alloy and glass powders. Different ratios were dispensed and mixed by the system. The mixing results are shown in Fig. 9. From the figure, it can be seen that both metal and glass powders distributed evenly and smaller copper alloy powders fully filled gaps between bigger glass powders after 5-minute mixing at a 60 r/min rotary speed. Table 3 illustrates the measured powder density at different powder mixing ratios and volume ratios of both materials. It can be seen that when the metal powder was more than glass powder (5 wt.% and 15 wt.%), the metal powder was the main constituent of the mixture. This was a metallic matrix composite (MMC). At 25 wt.% and 35 wt.% glass powder and copper alloy mixture, the volume ratio was in the range from 1:1 to 1:2. Both materials had nearly half of the mixture. Therefore, materials in this range would be the transition phase. As the volume ratio of metal and glass reduced, glass would start to dominate the mixture as the proportion of glass reached 45 wt.%. This type of materials was a ceramic matrix composite (CMC).

From Fig. 10, based on constant vibrational parameters and spherical powder shape of both powders, the flow rate of each type of powder was stable during the 600-sec dispensing testing. In Fig. 10 (a), due to the large differences of densities of copper alloy and glass, the flow rates reduced dramatically with the increasing glass proportion. Therefore, flow rates in volume were investigated to know the dispensed volume in unit time. As the orifice diameter dispensing pure copper alloy powders was 0.3 mm instead of 0.35 mm of dispensing for other types powders (this can be seen from Table 1), the volume flow rate of copper alloy for a 0.35 mm diameter nozzle can be higher. From Table 3, it can be seen that adding glass powders would reduce the flow rates gradually with the increasing of glass proportion until the glass proportion reached the transition phase. At the transition phase, when glass represented 25 wt.% or nearly 50 vol.% of the mixture, the flow rate reached the minimum. It started to increase after the transition phase even though glass proportion carried on increasing and reached the peak when the glass proportion was 65 wt.%. Pure glass had a lower flow rate.

The ratio of orifice diameter and the glass powder size was about 4

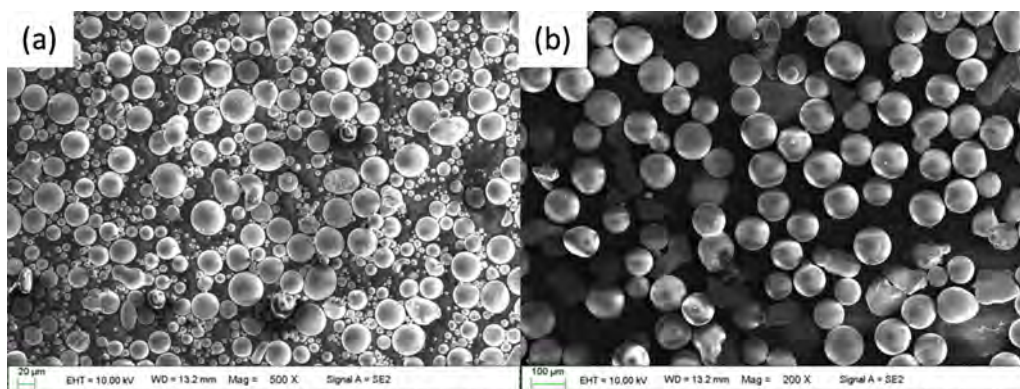


Fig. 6. SEM images of the powders used; (a) Cu10Sn powders and (b) soda-lime glass powders.

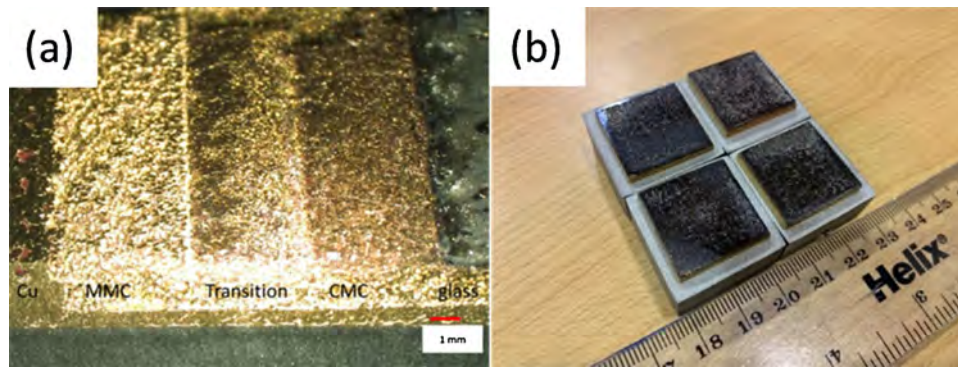


Fig. 7. Samples for mechanical property tests, (a) surface of the horizontal gradient sample for hardness tests, (b) vertical gradient samples for tensile and shear tests.

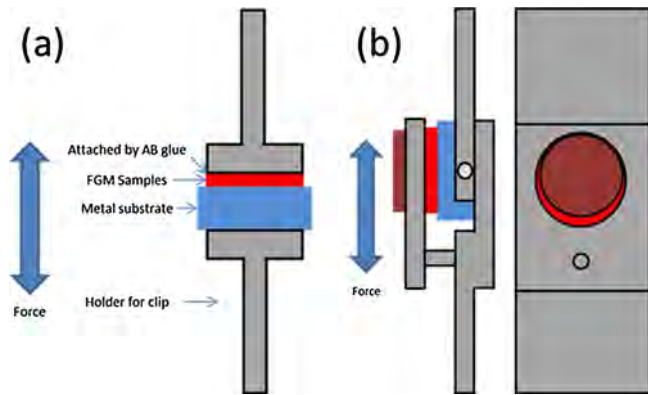


Fig. 8. Illustration of tensile and shear test specimen preparation, (a) tensile tests, and (b) shear tests.

whereas that of copper alloy was from 35 to 7 (the orifice diameter 0.35 mm and powder size from  $10\ \mu\text{m}$  to  $45\ \mu\text{m}$ ), so the glass powder flow rate would be much lower than that of the copper alloy powder in this case. Therefore, adding higher proportion of the glass powder would reduce the flow rates of the gradient mixture and it reached the lower limit when the ratio was 1:1. However, for CMC, the metal powder proportion reduced, *i.e.* smaller metal powders had more space for the vibration in the loose mixture. Therefore, the vibrated highly dense powders increased the downward dispensing force resulting in increasing flow rates. Meanwhile, the decreasing metal powders received more vibrational energy from the PZT and more vibrational space leading to higher dispensing force and higher flow rates. Therefore, the flow rates of CMC went up with metal powder proportion reducing.

#### 4.2. Printing of vertical gradient structure

A vertical gradient structure was built from pure copper alloy, MMC, transition, CMC to pure glass using the MMSLM system as shown

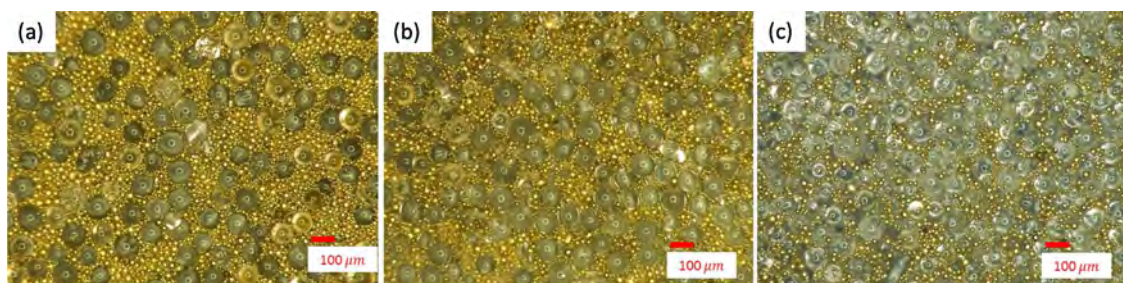


Fig. 9. Uniformity of different ratios after mixing, (a) metal matrix composite (15 wt.% glass), (b) the transition mixture (35 wt.% glass), and (c) ceramic matrix composite (65 wt.% glass).

Table 3

Measured results of each ratio of the gradient materials.

	Material (glass proportion)	Mixed powder density (g/ml)	Volume ratio between both materials (copper:glass)	Flow rate (mg/s)	Flow rate (ml/s)
Pure copper alloy	0 wt.%	5.15	–	11.9	2.31
MMC	5 wt.%	4.04	5.58:1	10.65	2.64
	15 wt.%	3.62	1.65:1	8.08	2.23
Transition	25 wt.%	3.25	1:1.15	5.23	1.61
	35 wt.%	2.83	1:1.85	5.12	1.81
CMC	45 wt.%	2.41	1:2.78	4.18	1.73
	55 wt.%	2.09	1:4.17	4.32	2.07
	65 wt.%	1.92	1:6.37	4.27	2.22
Pure glass	100 wt.%	1.5	–	2.78	1.85

in Fig. 11. Horizontal interface between metal and glass can also be achieved from the cross-section view.

The laser parameters are shown in Table 2. From Fig. 11, it was apparent that the amount of glass on the surface increased with the increase of glass ratio in the mixtures. On the top layer (Fig. 12 (e)), the glass surface was smooth and reflective. In Fig. 11, the glass part was not totally transparent and it looked dark. The black material can be speculated as the copper oxide or pure silicon (both are black in colour) that was generated during laser melting due to the following chemical reaction.

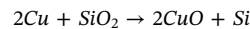


Fig. 12 shows the morphology of cross sections of the gradient structure. Similar to the surface views in Fig. 11, glass proportion increased and the copper reduced from lower to upper layers shown in Fig. 12. The solid copper alloy was printed as the base of the gradient structure. In the MMC section, metal component dominated with a certain proportion of glass. Pores can be seen in the glass parts from the transition phase to the pure glass in Fig. 12. Cracks also can be seen in the pure glass part after laser melting. Two reasons would cause this

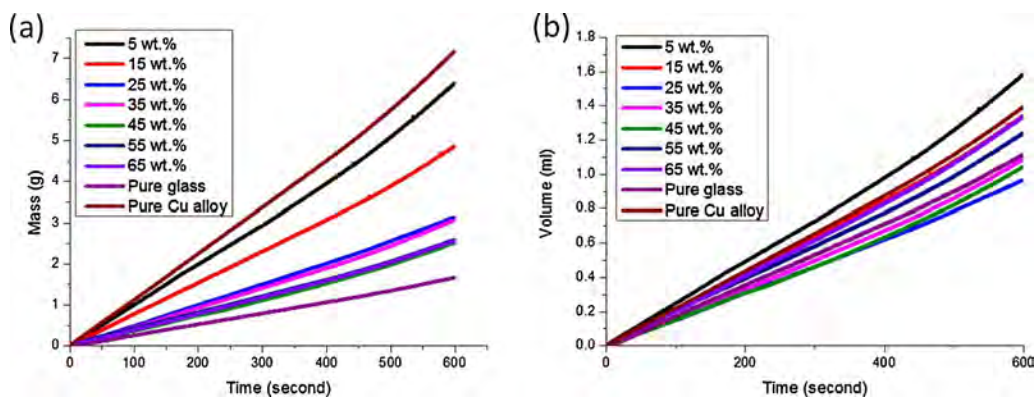


Fig. 10. Flow rates of different ratios of the mixtures, (a) in g/600 s, and (b) in ml/600 s.

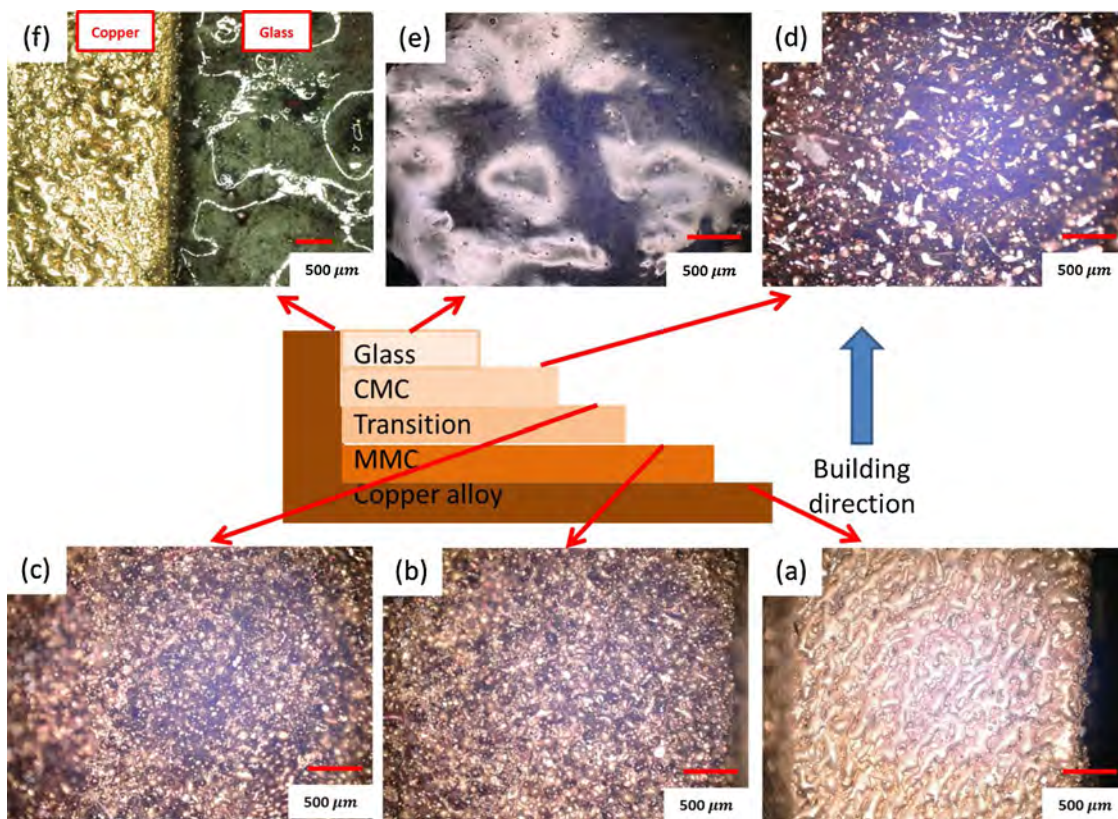


Fig. 11. Schematic of the vertical gradient structure and surface views for each powder ratio after laser melting, (a) metallic phase, (b) 15 % glass (MMC), (c) 35 % glass (transition phase), (d) 65 % glass (CMC), (e) glass phase, (f) the interface between the copper alloy and glass without FGM.

phenomenon. On the one hand, the thermal gradient in glass that has lower thermal conductivity resulted in different shrinkage rates during cooling down. Therefore, cracks occurred in the brittle material; on the other hand, it can be generated by the mismatch of coefficient of thermal expansion (CTE) between the glass and the lower CMC. This issue can be improved by increasing the gradient subdivision with higher glass proportion and further optimizing the laser parameters to reduce thermal gradient in the glass.

From Fig. 12, it can be concluded that the bottom pure copper alloy and the MMC phase were connected mainly by fused copper. By contrast, the connection between MMC part and the transition phase was formed by both fused metal and glass. Much more glass is distributed at the interface between the transition phase and the CMC part. In the glass zones, pure glass penetrated into the CMC section to form glass bonding for anchoring the top glass part. As soda-lime glass has low laser absorption and high (up to 80 %) transmission at the laser

wavelength [23], very limited laser energy can be absorbed directly by the glass powder grains. More heat came from the radiated copper alloy below because the laser went through the glass and heated the copper alloy in the CMC layers to generate a molten pool heated at least to 1000OC (the copper alloy melting point [24]). This temperature could soften or melt soda-lime glass in the molten pool and penetrated into the CMC section. The penetration played a role to anchor the glass, so that it did not distort after being quickly melted by the laser and cooled down. This is the main mechanism of combining glass with the gradient materials. When the thickness of the glass part was more than several millimetres, it was difficult to produce smooth and flat glass surface. Therefore, the method can generate large-size metal-glass parts. However, the thickness of glass was limited, which should be improved by further research.

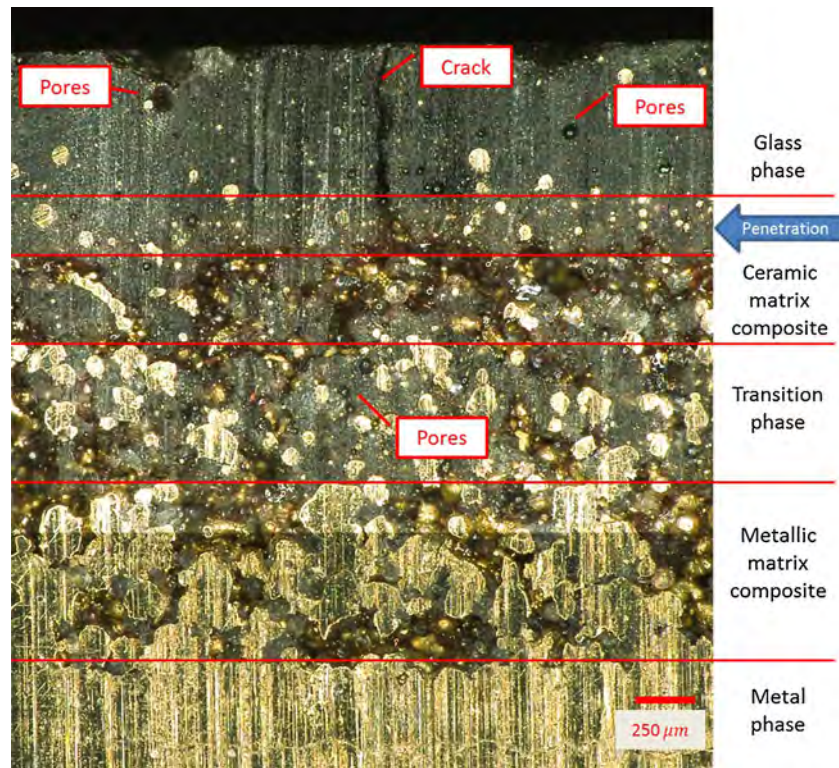


Fig. 12. Cross section view of the gradient structure by VHX-500 F optical microscope.

#### 4.3. Horizontal gradient structure

Metal-ceramic horizontal gradient structures cannot be built by normal SLM. However, by the MMSLM in this research this can be achieved. From the structure design shown in Fig. 13, it can be seen that the gradient structure is built both vertically and horizontally.

The gradient structure can be seen from Fig. 14(a) and (b). The surface was polished for a better observation. The vertical gradient structure had each layer on top with higher ratio of glass. The zones consisted of copper alloy, MMC, transition, CMC to glass. The horizontal gradient structures are similar.

#### 4.4. Micro structure of the processed gradient materials

SEM and EDS were used to observe the micro structure of the gradient sample cross section. Interfaces between two materials, copper alloy and glass, can be seen from the SEM images in Fig. 15 where more copper can be seen in the MMC zone and the interface was discrete and clear. Two materials were fused together by the laser to form the solid gradient material. From Section 4.2, copper oxide and pure silicon may be generated during laser melting. Based on Fig. 15 and the EDS image in Fig. 16, copper oxide layer between two materials cannot be detected. From the experience of the metal-ceramic joining mechanism in glass-to-metal joining technology, there would be an oxidation

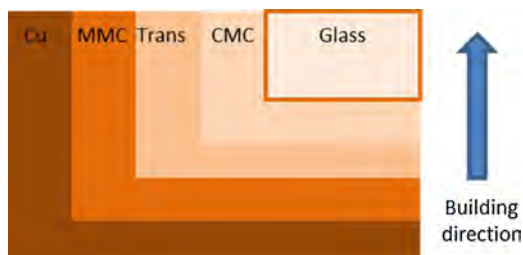


Fig. 13. Schematic of the horizontal gradient structure.

transition of several micron in thickness to connect glass and metal [10–12]. However, in this case, the oxide layer may be much thinner, probably in the nano scale, which requires further investigation using, e.g. Transmission Electron Microscopy (TEM).

SEM images of CMC cross section are shown in Fig. 17. Similar to that in the MMC zone, discrete interfaces between the two materials in CMC can be seen and there is also no oxide layers at the interface as shown in Fig. 18.

According to the micro images of both MMC and CMC, there was no metal oxide in the main body of the solid gradient materials. Two materials were fused together by the laser without an oxide layer as a transition layer.

#### 4.5. Mechanical properties

One advantage of FGM is the directional variation of mechanical properties. In order to know this effect, macro hardness indentation of different gradient materials was carried out and the results are shown in Fig. 19. From Fig. 20(a), as copper alloy is a ductile material, the indentation was totally plastic deformation. In (b), due to a certain proportion of glass, some brittle glass was crushed; however, the plastic indentation was still clear and regular. In Fig. 19 (c), there were both plastic deformation of the copper alloy and brittle fragmentation of glass at the indentation point. In Fig. 19 (d), brittle fragmentation of glass was much more than the metal plastic deformation. From (a) to (d), it can be obviously seen that the macro hardness indentation deformation changed gradually from a ductility to brittle due to the increasing proportion of soda-lime glass and the critical point occurred between the transition phase and the CMC phase. Fig. 20 is the hardness of each material. Copper alloy hardness was about 205 HV<sub>30</sub>. The FGMs had similar hardness as copper alloy at about 200 HV<sub>30</sub> even though glass proportion increased. This was because on one hand, more pores and cracks in the FGMs could reduce the hardness; on the other hand, glass beads broken by the indentation could enlarge the size of the indenter and the impression, which led to a lower hardness.

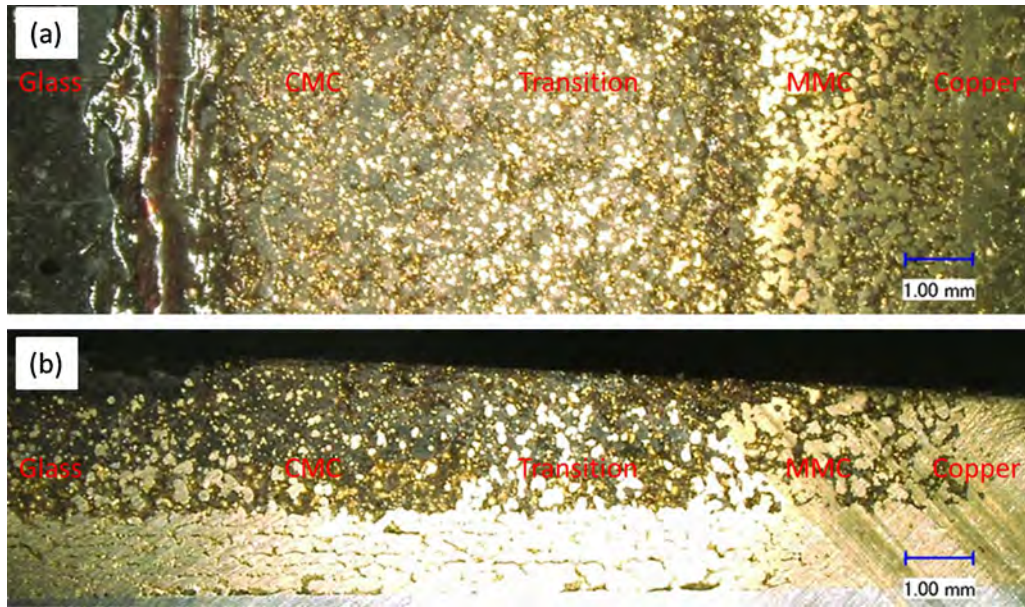


Fig. 14. Optical images of the horizontal gradient structure, (a) the top view, and (b) the cross section view.

Hardness of pure glass was about 277 HV<sub>30</sub> that was much higher than the other four values. Similarly, glass hardness was not as much as a solid glass (generally 439–484 HV) [24] due to the existence of micropores and cracks.

Tensile test and shear test were carried out to understand the strength characteristics of the solid gradient structures. Both samples were broken between the transition phase and the CMC phase in the tensile tests and shear tests as shown in Fig. 21. This can be confirmed by comparison of the surfaces of different type of the mixtures according to images in Figs. 11 and 21. There were more copper alloy in the transition zone (Fig. 24 (a)), and glass dominated the CMC surface in Fig. 21 (b). This means that the metal-glass gradient structure is weakest at the bonding interface of the transition phase and CMC phase, which was the critical point from ductility to brittleness.

Fig. 22 shows the results of the tensile and shear tests. In the tensile test (Fig. 22 (a)), the strength went up quickly after a slight increasing until it reached the peak of 0.874 MPa and the corresponding displacement was about 92.44  $\mu\text{m}$ . Compared with tensile tests, the shear tests graph experienced a continuous gradual increasing until the break occurred at about 0.819 MPa. From both graphs, it can be seen that ductile deformation was the main characteristic before breaking and the peak was the connecting strength between ductile and brittle phases.

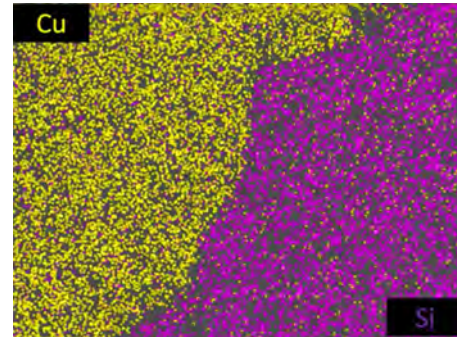


Fig. 16. The EDS image of Fig. 17 (b).

#### 4.6. Demonstration samples

A multi-material heart ring was made by the method as a demonstration in Fig. 23. The inner heart and the outer heart ring were made by glass, built vertically from pure copper alloy, gradient materials to pure glass. The middle ring was made by pure copper alloy. The surface was polished for clear observation. It can be seen that the glass part had big pores and some contaminated metal powders. In Fig. 24, a 'LPRC' logo was printed horizontally with the gradient materials. Each letter

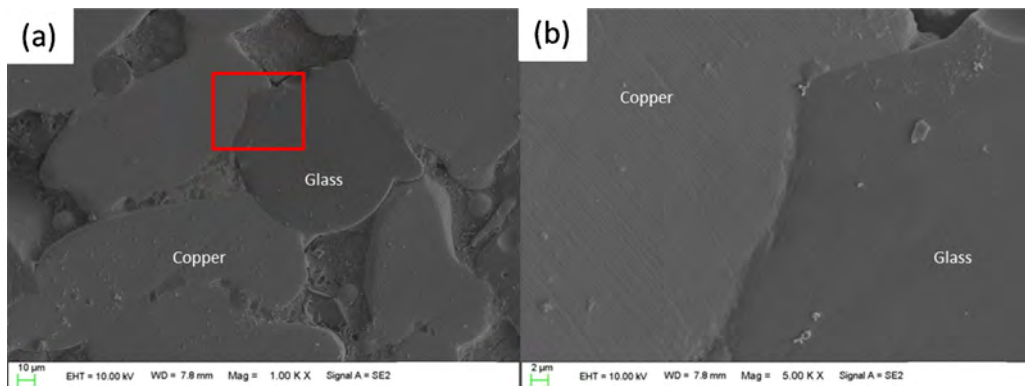


Fig. 15. SEM images of the cross sections of the MMC parts; (a) SEM images and (b) higher magnitude of the red box in (a). (For interpretation of the references to colour in this figure legend, the reader is referred to the web version of this article).

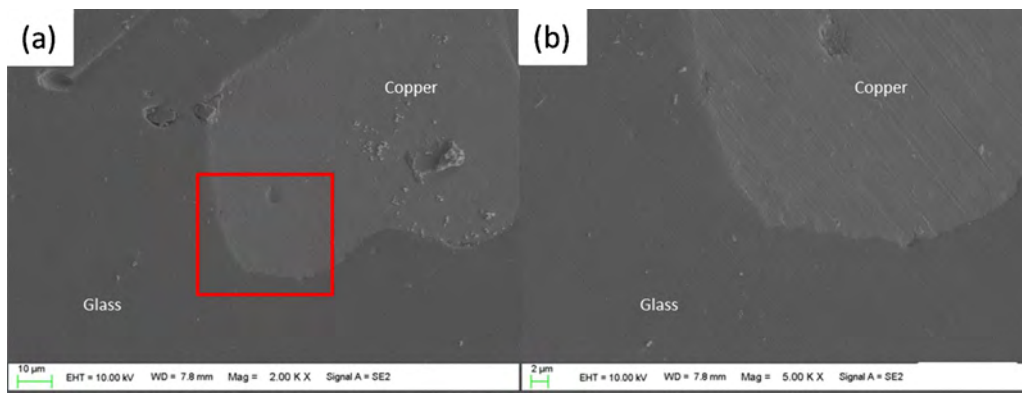


Fig. 17. SEM images of the cross sections of the CMC parts; (a) SEM images and (b) higher magnification of the red box in (a). (For interpretation of the references to colour in this figure legend, the reader is referred to the web version of this article).

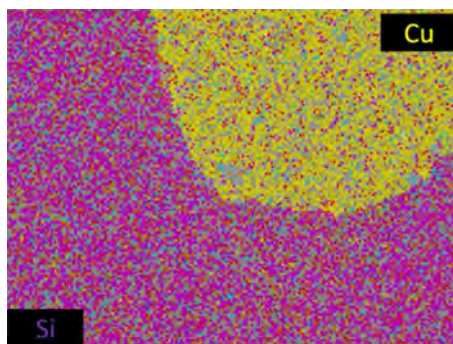


Fig. 18. EDS image of Fig. 19(b).

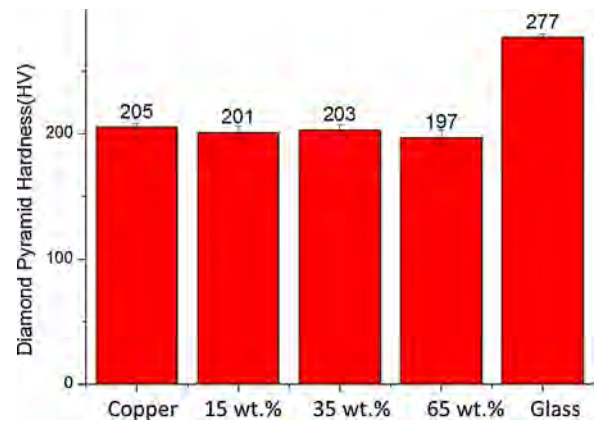


Fig. 20. Hardness of different ratios of the gradient materials.

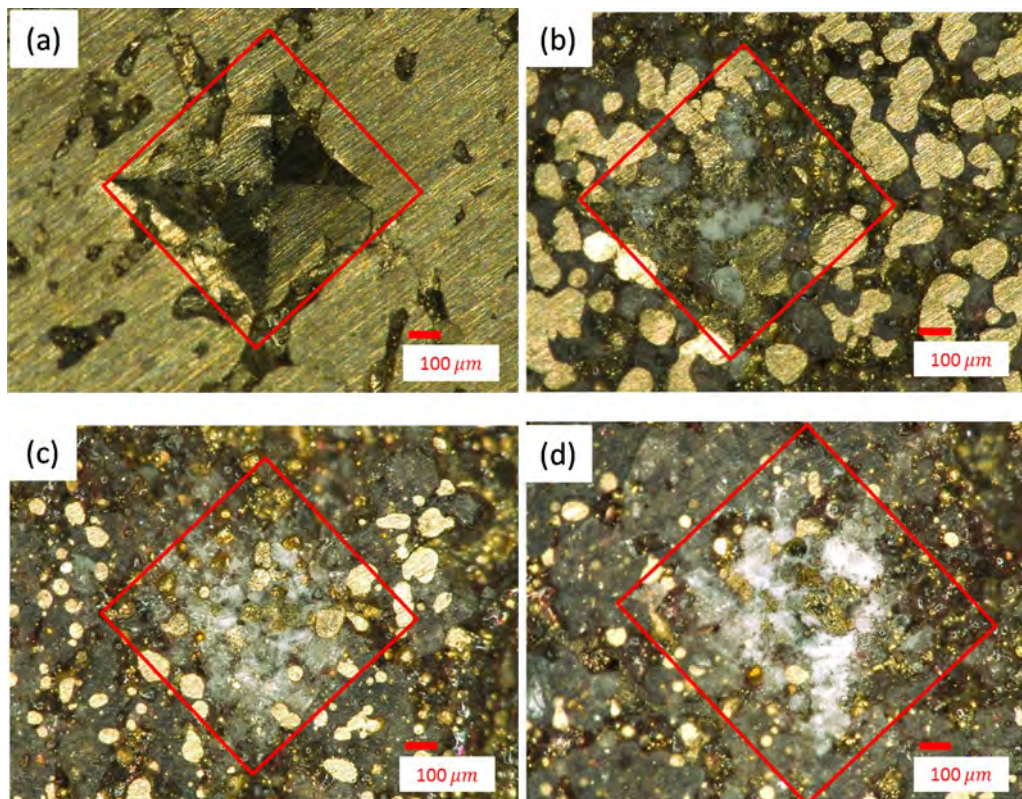


Fig. 19. Images of indentation of each ratio of materials, (a) pure copper, (b) MMC, (c) the transition phase, (d) the CMC.

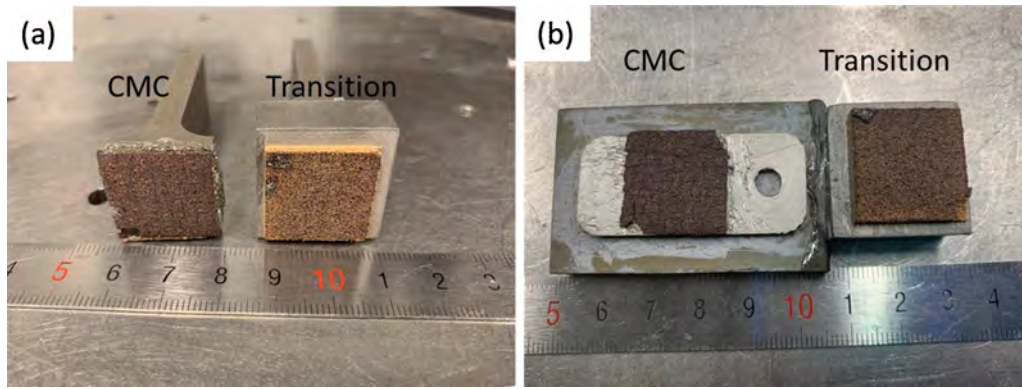


Fig. 21. Samples after tensile and shear tests, (a) tensile tests, and (b) shear tests.

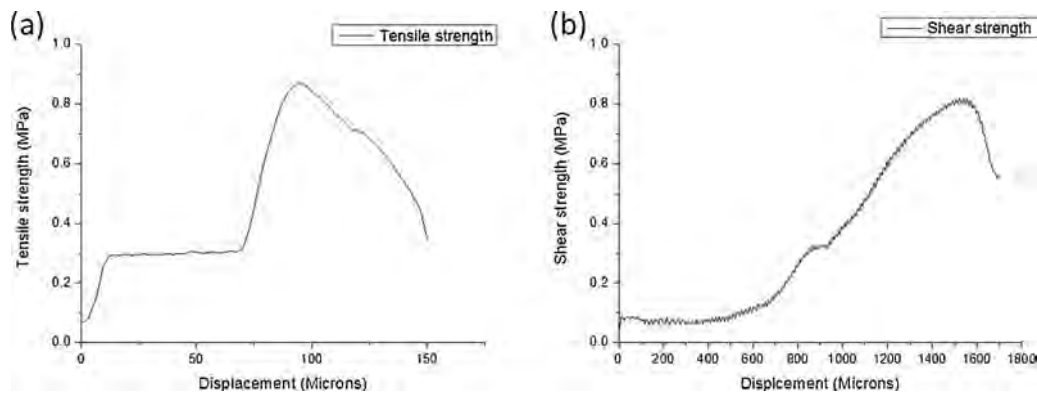


Fig. 22. Results of (a) the tensile tests, and (b) the shear tests.

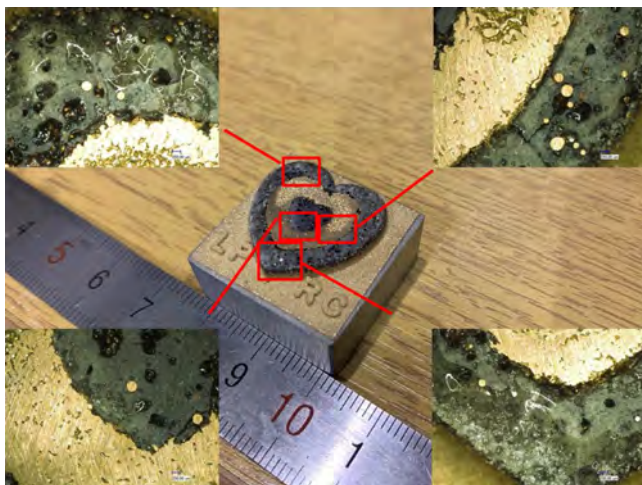


Fig. 23. A dual-heart sample fabricated by the method.

was made by MMC, the transition phase, CMC, and the glass section horizontally respectively to show the horizontal gradient structure.

5. Conclusions

In order to improve bonding between metal and glass in the multi-material SLM parts (metal/glass), FGMs were applied as the transition zones from pure metal to pure glass. A designed *in situ* powder mixing system was made for mixing the metal and glass powders at various ratios. Powders were dispensed onto the work platform via a powder feeding nozzle using ultrasonic vibration. Based on 600-second measurements using an electric balance, the powder flow rate for each powder mixing ratio was obtained. The flow rates reduced with the

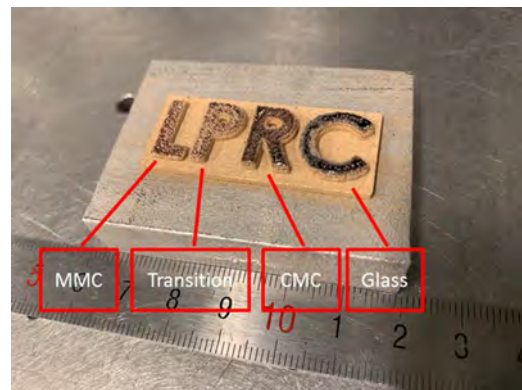


Fig. 24. 'LPRC' letters with horizontally distributed gradient materials.

glass proportion increasing until the transition phase that had the lowest flow rates. The flow rates would increase with increasing glass proportion in the CMC because decreasing highly dense metal powders received more vibrational energy and space to accelerate the flow. All flow rates were constant and stable during dispensing based on stable parameters and spherical powder shape.

The bonding mechanism of metal and glass was that melted glass penetrated into the CMC phase, which played a role to anchor the glass, so that it did not distort after being quickly melted by the laser and cooling down. Both horizontal gradient and vertical gradient structures were achieved by this method. According to SEM and EDS images of both MMC and CMC, materials were fused together and discrete interfaces between two materials were clearly seen without oxidation transition layers between materials.

The indentation deformation of each ratio also gradually changed from a ductile to a brittle phase. In both tensile and shear tests, the

fractures occurred at the interface between the transition zone and the CMC zone, which was also the transition from ductile to brittle phases.

#### Declaration of Competing Interest

None.

#### Acknowledgements

Wei and Chueh acknowledge the support of their PhD research by The University of Manchester PGR scholarships. Yan and Li are grateful for the Leverhulme Trust visiting professorship (VP1-2018-022) and the Royal Society Wolfson Research Merit award (2014/R1).

#### References

- [1] X. Zhang, C. Wei, Y.-H. Chueh, L. Li, An integrated dual ultrasonic selective powder dispensing platform for three-dimensional printing of multiple material Metal/Glass objects in selective laser melting, *J. Manuf. Sci. Eng.* 141 (1) (2019) 011003.
- [2] O. Al-Jamal, S. Hinduja, L. Li, Characteristics of the bond in Cu-H13 tool steel parts fabricated using SLM, *CIRP Ann. Manuf. Technol.* 57 (1) (2008) 239–242.
- [3] C. Wei, L. Li, X. Zhang, Y.-H. Chueh, 3D printing of multiple metallic materials via modified selective laser melting, *CIRP Ann.* 67 (1) (2018) 245–248.
- [4] S. Matsusaka, M. Urakawa, H. Masuda, Micro-feeding of fine powders using a capillary tube with ultrasonic vibration, *Adv. Powder Technol.* 6 (4) (1995) 283–293.
- [5] S. Matsusaka, K. Yamamoto, H. Masuda, Micro-feeding of a fine powder using a vibrating capillary tube, *Adv. Powder Technol.* 7 (2) (1996) 141–151.
- [6] X. Lu, S. Yang, J.R. Evans, Studies on ultrasonic microfeeding of fine powders, *J. Phys. D Appl. Phys.* 39 (11) (2006) 2444.
- [7] L. Qi, X. Zeng, J. Zhou, J. Luo, Y. Chao, Stable micro-feeding of fine powders using a capillary with ultrasonic vibration, *Powder Technol.* 214 (2) (2011) 237–242.
- [8] M. Fateri, A. Gebhardt, Selective laser melting of soda-lime glass powder, *Int. J. Appl. Ceram. Technol.* 12 (1) (2015) 53–61.
- [9] R. Khmyrov, C. Protasov, S. Grigoriev, A. Gusarov, Crack-free selective laser melting of silica glass: single beads and monolayers on the substrate of the same material, *Int. J. Adv. Manuf. Technol.* 85 (5-8) (2016) 1461–1469.
- [10] T.-S. Chern, H.-L. Tsai, Wetting and sealing of interface between 7056 Glass and Kovar alloy, *Mater. Chem. Phys.* 104 (2-3) (2007) 472–478.
- [11] R. Joshi, R. Chhibber, Development and interface characterization of unmatched glass-metal joint, *J. Manuf. Process.* 31 (2018) 787–800.
- [12] M. Mantel, Effect of double oxide layer on metal–glass sealing, *J. Non. Solids* 273 (1-3) (2000) 294–301.
- [13] G. Udupa, S.S. Rao, K. Gangadharan, Functionally graded composite materials: an overview, *Procedia Mater. Sci.* 5 (2014) 1291–1299.
- [14] S. Howard, Y. Tsui, T. Clyne, The effect of residual stresses on the debonding of coatings—I. A model for delamination at a bimaterial interface, *Acta Metall. Mater.* 42 (8) (1994) 2823–2836.
- [15] A. Gupta, M. Talha, Recent development in modeling and analysis of functionally graded materials and structures, *Prog. Aerosp. Sci.* 79 (2015) 1–14.
- [16] C. Han, Y. Li, Q. Wang, D. Cai, Q. Wei, L. Yang, S. Wen, J. Liu, Y. Shi, Titanium/hydroxyapatite (Ti/HA) gradient materials with quasi-continuous ratios fabricated by SLM: material interface and fracture toughness, *Mater. Des.* 141 (2018) 256–266.
- [17] J. Ma, G. Tan, Processing and characterization of metal–ceramics functionally gradient materials, *J. Mater. Process. Technol.* 113 (1-3) (2001) 446–449.
- [18] S. Nai, M. Gupta, Influence of stirring speed on the synthesis of Al/SiC based functionally gradient materials, *Compos. Struct.* 57 (1-4) (2002) 227–233.
- [19] E. Olakanmi, Selective laser sintering/melting (SLS/SLM) of pure Al, Al–Mg, and Al–Si powders: effect of processing conditions and powder properties, *J. Mater. Process. Technol.* 213 (8) (2013) 1387–1405.
- [20] D. Jha, T. Kant, R. Singh, A critical review of recent research on functionally graded plates, *Compos. Struct.* 96 (2013) 833–849.
- [21] S. Kumar, J.-P. Kruth, Composites by rapid prototyping technology, *Mater. Des.* 31 (2) (2010) 850–856.
- [22] S. Yang, J.R. Evans, A multi-component powder dispensing system for three dimensional functional gradients, *Mater. Sci. Eng. A* 379 (1-2) (2004) 351–359.
- [23] S. Karazi, I. Ahad, K. Benyounis, Laser Micromachining for Transparent Materials, (2017).
- [24] M.F. Ashby, *Materials and the Environment: Eco-informed Material Choice*, Elsevier, 2012.